Paper # 07F-67 **Topic:** Diagnostics SAND2007-6249C

2007 Fall Meeting of the Western States Section of the Combustion Institute
Sandia National Laboratories, Livermore, CA
October 16 & 17, 2007.

Investigation of photolytic interferences in nanosecond and picosecond excitation schemes for two-photon laser-induced fluorescence imaging of atomic hydrogen in flames

Waruna D. Kulatilaka, Brian D. Patterson, Jonathan H. Frank and Thomas B. Settersten

Combustion Research Facility, Sandia National Laboratories, Livermore, CA 94551

Detection of atomic hydrogen in flames and plasmas requires multi-photon excitation schemes because single-photon excitation in the vacuum ultraviolet (VUV) is impractical in these optically thick environments. Quantitative measurement of atomic hydrogen in flames using two-photon-excited laser-induced fluorescence (TP-LIF) is complicated by photolytic interference and rapid loss of excited-state population via stimulated emission. We investigate the sources of photolytic interference and the effects of stimulated emission using nanosecond and picosecond lasers for TP-LIF line imaging of atomic hydrogen in premixed methane/air, hydrogen/oxygen and hydrogen/air flames. A laser beam at 205 nm is used for two-photon excitation of the (n=1 $\rightarrow\rightarrow$ n=3) transitions of atomic hydrogen. Line images of the LIF signal from the (n=3 $\rightarrow$ n=2) transitions at 656 nm are recorded using a state-of-the-art intensified CCD camera. Stimulated emission is monitored using a fast PIN photodiode. Signals produced by picosecond and nanosecond excitation are directly compared for a range of flame conditions, and recommendations for optimal detection are presented.

1 Introduction

Elemental hydrogen is a principal constituent of a majority of combustion fuels. Chemical reactions involving atomic hydrogen play a significant role in combustion and energy transfer processes involving these fuels because of the high reactivity and diffusivity of hydrogen atoms. Numerous laser-based diagnostic techniques, such as laser-induced fluorescence [1–6], polarization spectroscopy [7], wave-mixing techniques [8], and stimulated emission (SE) [9, 10], have been developed and applied to measure spatially resolved atomic hydrogen concentration profiles in reacting flows. Among these, LIF is the most widely used and most easily implemented diagnostic technique. Obtaining quantitative concentrations from the measured LIF signals, however, is often complicated by processes such as collisional quenching, photoionization, stimulated emission (SE), saturation and Stark shifting, photolytic production of atomic hydrogen by the probe laser beam and broadband fluorescence interferences from other flame species [11,12]. Thus, it is essential to avoid or apply appropriate signal corrections for each of these processes in order to obtain quantitative H-atom concentrations.

Detecting atomic hydrogen in flames and plasmas often involves multi-photon excitation schemes. All single-photon transition frequencies from the ground state to electronically excited states of

atomic hydrogen lie in vacuum ultraviolet (VUV). Single-photon excitation schemes are not feasible in practical combustion environments because the medium is optically thick to VUV photons. Instead, excitation wavelengths can be shifted to the ultraviolet (UV) region using various multi-photon schemes, as demonstrated in the past [13, 14]. A selection of multi-photon excitation schemes for LIF detection is shown in Figure 1. The simplest and most widely used scheme employs two 205-nm photons for (n=1→→n=3) pumping and fluorescence detection from the H_α transition (n=3 → n=2) at 656 nm. This scheme requires only one laser beam, and the fluorescence signal is generated at a discrete wavelength that is well separated from the pump laser.

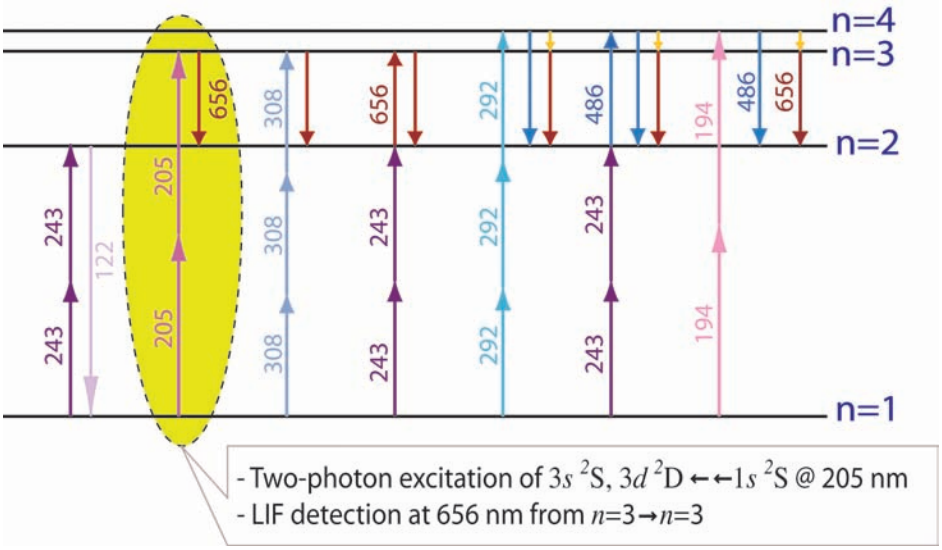

Figure 1: Multi-photon excitation LIF schemes for detecting atomic hydrogen.

The multi-photon excitation schemes shown in Figure 1 require high-intensity UV laser pulses to generate sufficient LIF signal because two- or three-photon absorption cross sections are significanlty smaller than the corresponding single-photon absorption cross sections. The high-intensity UV laser pulses can give rise to several of the complexities listed above. The photolytic production of H-atoms that results from photodissociation of certain flame constituents can be particularly problematic because the species being probed is created by the probe laser itself. Goldsmith [15] studied for the first time photochemical effects of 205-nm TP-LIF detection of atomic hydrogen using a conventional nanosecond laser system. The author reported photodissociation of water vapor in the post flame region as primary cause of photolytic creation of H-atoms. In addition to photodissociation of vibrationally excited water vapor, Gasnot et al. [16] identified CH_3 radical as an important photolytic precursor of atomic hydrogen in the reaction zone of low-pressure methane/air flames. It has been reported that absorption of 205-nm photons by formyl (HCO), carboxyl (-COOH), vinyl (C_2H_3) and allyl (C_3H_5) radicals also can produce hydrogen atoms [17]. Studies of photochemical effects in 205-nm TP-LIF detection of atomic hydrogen in multiple species fluorescence imaging in hydrogen-nitrous oxide flames [18] and 243-nm TP-LIF [9] have also been reported.

Stimulated emission is a laser-dependent loss mechanism for the excited state, and its effect further complicates the quantification of TP-LIF signals. In single-step, two- or three-photon excitation

schemes, a significant population inversion can occur between the upper electronic state and intermediate electronic state(s). Spontaneously emitted photons can readily stimulate emission from the excited atoms, resulting in a potentially significant loss mechanism for the fluorescence measurement. The efficiency of this loss mechanism depends nonlinearly on the density and spatial distribution of the excited atoms. At high laser intensities, which produce large population inversion on a short time scale, SE can be a particularly effective mechanism for population loss from the excited state that potentially limits the fluorescence yield. It should be noted that population inversion (thus SE) does not take place in two-step excitation schemes [3] where significant population is pumped into the intermediate level by the two-photon pump step.

Other complexities, such as photoionization and broadband interferences, in the 205-nm excited TP-LIF scheme are relatively small or negligible at low and moderate laser intensities, as verified by our current work. In the 205-nm TP-LIF scheme, the fluorescence signal at 656 nm is well separated from the strongest broadband interferences, which occur in the blue-green part of the spectrum. Additionally in flames, the Doppler width of the hydrogen lines is significantly larger than the laser linewidth, and Stark shifting at higher laser intensities have little effect on the fluorescence signal.

When TP-LIF measurements are performed in a non-saturating regime using relatively low laser intensity, a simple rate-equation model can be used to obtain quantitative concentration from the measured LIF signal, provided proper quenching corrections are made [16]. As with any non-saturated LIF-based technique, poorly characterized electronic quenching remains a significant complication to quantitative measurements. To operate in this regime, a quadratic dependence of the fluorescence signal on the laser intensity is a necessary condition. However, this criterion alone is not sufficient because a combination of photochemical effects and laser-dependent loss (ionization or SE) could still result in near-quadratic signal dependence on the laser intensity. Furthermore, photochemical interferences depend on the local temperature and species concentration [19], a point that is critical in evaluating the significance of interference in two-dimensional imaging of atomic hydrogen in flames.

In an earlier study, Settersten et al. [20] reported significant advantages of using picosecond-duration (ps) laser pulses instead of traditionally used nanosecond-duration (ns) pulses for TP-LIF of atomic oxygen in methane/air flames. Because the TP-LIF signal generation involves two-photon absorption, to generate the same fluorescence signal level, ps excitation requires significantly less pulse energy than is required for ns excitation. For atomic oxygen detection, Settersten et al. [20, 21] demonstrated that the photolytic production of atomic oxygen is caused by a single-photon process, and is therefore scales linearly with the laser pulse energy. As a result, the contribution of photolytic interference was significantly reduced when using ps excitation as compared to ns excitation for TP-LIF detection of atomic oxygen. Based on these results, Frank and Settersten [19] succesfully demonstrated interference-free planar laser induced fluorescence (PLIF) imaging of atomic oxygen in steady and unsteady laminar premixed methane flames. In the current study, we use a similar approach to investigate the ns and ps excitation schemes for TP-LIF detection of atomic hydrogen in flames.

2 Experimental Apparatus and Procedure

In the current study, one-dimensional line images of atomic hydrogen are produced by imaging the 656-nm fluorescence produced by two-photon excitation at 205 nm. Images were produced in premixed methane and hydrogen flames. Premixed methane/oxygen/nitrogen ($CH_4/O_2/N_2$), hydrogen/oxygen (H_2/O_2), and hydrogen/oxygen/nitrogen ($H_2/O_2/N_2$) flames were studied for a range of flame equivalence ratios. Imaging the H-atom fluorescence profile along the radial direction of the axi-symmetric laminar flame enabled the characterization of the photochemical effects taking place across a wide thermal and species concentration gradient. Line images were recorded for a range of laser energies in each flame. SE signals were also monitored in the forward-propagation direction of the laser. Direct comparison of the shape of the line images in a given flame enabled the determination of interference-free detection limits for ns and ps excitation schemes at each flame condition. The effects of SE for each excitation scheme can also be compared.

The experimental apparatus is shown in Figure 2. Similar to our previous O-atom LIF studies [21], the apparatus includes a tunable nanosecond laser system, a tunable picosecond laser system, an axi-symmetric premixed flame, and an intensified CCD camera for line imaging.

The nanosecond laser system consists of a tunable dye laser (Continuum Model ND6000) pumped by the second harmonic of an injection-seeded Nd:YAG laser (Continuum Model Precision PRO 9020) operating at 20 Hz. The final amplifier of the ND6000 was bypassed and the output beam from ND6000 was amplified by passing through an external pulsed dye amplifier (PDA) to obtain stable laser pulses with a significantly improved spatial beam profile. The PDA consists of a side-pumped dye cell and the pump beam originated from the second harmonic of the same Nd:YAG laser. Solutions of Sulforhodamine 640 laser dye in methanol were used in ND6000 and PDA to generate laser radiation at 615.4 nm. The 615.4-nm output was frequency tripled using two β-barium borate (β-BBO) crystals to generate ultraviolet (UV) radiation at 205.14 nm. The maximum UV pulse energy at the probe volume was approximately 1.5 mJ/pulse, and the pulse duration was approximately 3.5 ns.

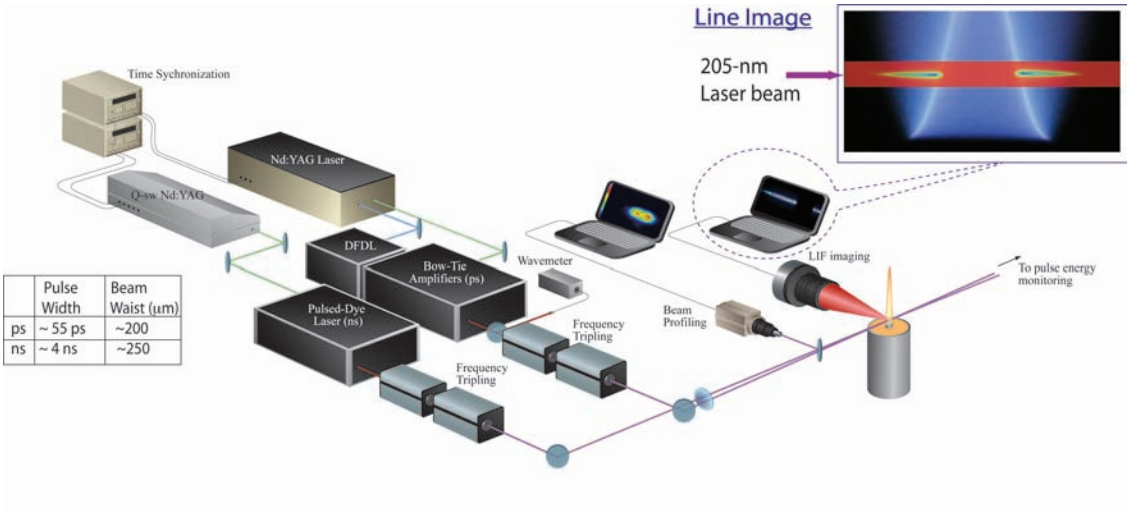

Figure 2: Experimental Apparatus.

The picosecond laser system consists of a distributed-feedback dye laser (DFDL) pumped by the third harmonic of a Nd:YAG laser (Coherent Model Infinity) operating at 20Hz. The weak DFDL pulses are amplified using two bow-tie amplifiers pumped by the second harmonic of the same Nd:YAG laser. The construction and operation of the DFDL system is described in detail elsewhere [22]. The DFDL system generates Fourier-transform-limited laser radiation with a pulse duration of approximately 55 ps. The DFDL and the bow-tie amplifiers were operated using solutions of Sulforhodamine 640 laser dye in methanol to generate laser radiation at 615.4 nm and subsequently frequency tripled to generate UV radiation at 205.14 nm. The maximum UV pulse energy was approximately 0.3 mJ/pulse.

The ns and ps beams were focused and crossed above the axi-symmetric burner using two 1-m focal length UV lenses. The beam diameters of ns and ps beams at the probe volume were approximately 250 μm and 200 μm, respectively, and did not vary appreciably across the flame. The spatial beam profile of each beam at the probe volume was nearly top-hat and was monitored by imaging onto a beam profiling camera on a frequent basis during the experiment. After passing through the flame, the two UV beams were reflected by a 205-nm dichroic mirror and down-collimated onto two joulemeters (Molectron Model J3-05) to monitor the intensity of each laser beam. At higher laser energies, SE signal from n=3$\rightarrow$ n=2 was observed at 656 nm along the direction of the laser beams. The SE signal was monitored behind the 205-nm dichroic mirror by focusing onto a PIN photodiode. A BK7 glass flat and a 656-nm H_α filter was placed in front of the photodiode to block residual UV radiation and scattered light. At the highest laser intensities, and particularly in rich H_2 flames, the SE signal was easily visible by the naked eye.

Fluorescence signal from the n=3 $\rightarrow$ n=2 transitions of atomic hydrogen was imaged onto an intensified CCD camera using a combination camera lenses. Two identical camera lenses were used in a back-to-back configuration at infinite conjugate ratio to collect and image the fluorescence on the intensifier. A 656-nm H_α filter was placed in between the two camera lenses, where the collected light is roughly collimated. The CCD camera (PixelVision) was equipped with a Gen III image intensifier. The LIF line image from first half of the axi-symmmetric flame was recorded.

Table 1 summarizes the premixed $CH_4/O_2/N_2$ flames investigated currently. The exit nozzle diameter of the burner used for CH_4 flames was 6 mm. Flow rates were selected such that the height of the inner cone of the flame remained approximately the same. Two types of H_2 flames were also investigated. Characteristics of the premixed H_2/O_2 and $H_2/O_2/N_2$ flames are given in Tables 2 and 3, respectively. These flames were operated on a burner having exit nozzle diameter of 2 mm. $H_2/O_2/N_2$ flames are representative of H_2/Air flames.

LIF line images were recorded using the ns laser and ps laser separately for a range of laser intensities. Between 8 and 4000 laser shots were accumulated on the CCD chip, and up to 200 frames were averaged to improve the signal-to-noise ratio (SNR) so that slight changes in the line image could be detected. The two-dimensional LIF images were converted to line images by integrating the detected counts in the vertical direction (perpendicular to the laser propagation direction). In the vertical direction, the LIF intensity profile was approximately Gaussian, with a full-width at half maximum of approximately five pixels. The resulting line images maintained the full spatial resolution provided by the imaging system in the radial direction of the flame; each pixel corresponded to approximately 25 μm in the flame. In the following, peak-normalized LIF profiles are plotted for the range of laser energies studied to facilitate observation of changes in the shape of

the profile, which is indicative of photolytic interference or SE. Because only the *changes* of the shape of relative LIF radial profile are important, no quenching corrections were necessary.

Table 1: Premixed $CH_4/O_2/N_2$ Flame Conditions.

Φ	T_{ad} (K)	CH_4 (slm)	O_2 (slm)	N_2 (slm)	Flame
0.50	2407	0.657	2.623	2.644	Flame1
0.70	2512	0.780	2.210	3.374	Flame2
1.00	2602	0.830	1.650	3.272	Flame3
1.20	2591	0.900	1.500	3.019	Flame4
1.50	2539	0.998	1.336	2.056	Flame5
1.80	2431	1.000	1.111	1.144	Flame6

Table 2: Premixed H_2/O_2 Flame Conditions.

Φ	T_{ad} (K)	H_2 (slm)	O_2 (slm)	Flame
0.25	2500	1.956	3.913	H2Flame025
0.75	3043	4.211	2.806	H2Flame075
1.00	3079	5.610	2.806	H2Flame100
1.25	3060	5.962	2.384	H2Flame125

Table 3: Premixed $H_2/O_2/N_2$ Flame Conditions.

Φ	T_{ad} (K)	H_2 (slm)	O_2 (slm)	N_2 (slm)	Flame
0.62	1874	0.620	0.505	1.875	H2AirFlame062
1.00	2386	1.480	0.747	2.773	H2AirFlame100

3 Results and Discussion

3.1 Methane Flames

Nanosecond and picosecond excitation schemes were investigated in six different methane flames ($CH_4/O_2/N_2$) with equivalence ratio ranging between 0.50 - 1.80 as shown in Table 1. The adiabatic flame temperature of these flames are in the range of approximately 2400 K - 2600 K. Peak-normalized LIF signals for four of the six $CH_4/O_2/N_2$ flames recorded using the picosecond and nanosecond laser excitation schemes are shown in Figure 3 and Figure 4, respectively. The signals are plotted as a function of the radial position in the flame, and only the left half of the axi-symmetric flame is shown. In each flame, LIF line images were recorded for approximately 12 different laser pulse energies between the minimum (dark-blue curve) and maximum (red curve)

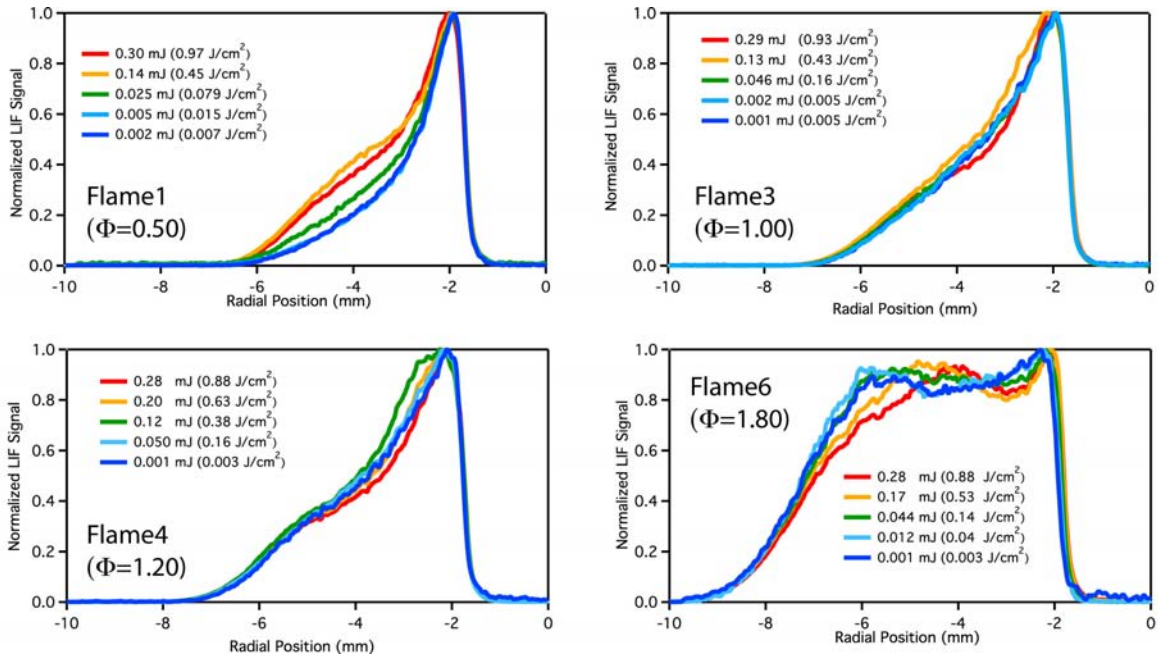

Figure 3: Methane Flames - Picosecond Excitation Scheme.

laser energies. For clarity, profiles for only five of the laser energies are shown in each frame in Figures 3 and 4. At the minimum laser energy used in each case, a signal-to-noise ratio (SNR) of approximately 4 could be obtained in the region corresponding to the flame front. For this lowest-energy-case, the above SNR was estimated in a ten-frame averaged image where each frame is exposed to 400 laser shots. In each scheme, the laser energy was varied in relatively small steps starting from the lowest energy until a change in the relative H-atom profile is noticed. For each case, the profile obtained with the highest laser energy for which no profile distortion is observed is shown by the light-blue curve.

The types of profile distortions observed in Figures 3 and 4 can be broadly categorized in to three groups. In the first group, a systematic change in the relative H-atom profile occurs on the product side of the flame, as seen in the lean (ϕ = 0.50) flame with ps-excitation and in lean to moderately-rich (ϕ = 0.50 – 1.20) flames with ns-excitation. For both excitation schemes, this type of profile distortion is more prominent in lean flames. In lean flames, the ratio of the number density of water vapor to that of atomic hydrogen is significantly higher than in rich flames. Thus, the relative interference resulting from H_2O dissociation will be more pronounced in leaner flames. Furthermore, the location of the profile distortion (product side of the flame) is consistent with the creation of H-atoms by photodissociation of vibrationally-excited water molecules [15].

The second type of profile distortion is seen in moderately-rich flames (ϕ = 1.20 and 1.50) with ps-excitation and in rich flames (ϕ = 1.50 and 1.80) with ns-excitation. In this case, a change in profile shape occurs in the vicinity of the flame front, consistent with the production of atomic hydrogen via photodissociation of flame radicals in the reaction zone. Desgroux et al. [16, 23] indicate that small hydrocarbon radicals, mainly methyl radical (CH_3), can photodissociate by absorbing a 205-nm photon, and thus can photolytically produce H-atoms.

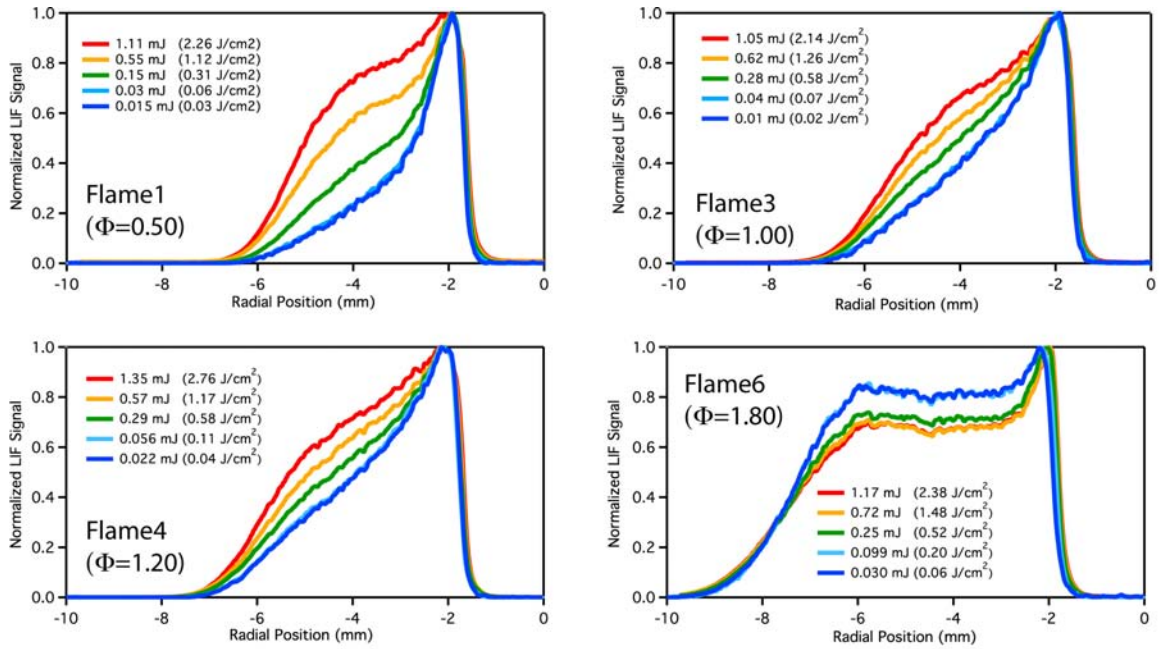

Figure 4: Methane Flames - Nanosecond Excitation Scheme.

The third type of profile distortion is mainly seen with ps-excitation scheme in rich methane flames (ϕ = 1.00 – 1.80) and also very clearly seen in stoichiometric and rich hydrogen flames (as discussed in Section 3.2). In this case, as the excitation energy is increased, the LIF signal in the products region decreases relative to that at the peak location, resulting an effective narrowing of the relative atomic hydrogen profile. This effect is most pronounced in the stoichiometric H_2/O_2 flame, and a similar behavior was observed in measurements of atomic oxygen in H_2/O_2 flames [21]. We postulate that this distortion is caused by the spatially non-uniform population loss resulting from SE. In fact, at these experimental conditions we observed strong SE signals which could be easily seen by the naked eye. The significantly higher atomic hydrogen number density in the rich flames enables the population loss mechanism that leads to SE growth to effectively compete with very efficient collisional quenching process. If the SE initiates from spontaneous emission in the region of highest density of excited-state hydrogen atoms (ie. flame front), as it propagates away from the flame front, the SE intensity will grow nonlinearly, and thus can more effectively deplete the excited-state population in the flame products region. In this picture, the LIF signal will experience a spatially non-uniform depletion. This behavior is consistent with our experimental observations where, in atomic-hydrogen-rich flames, the LIF signal in the products region decreases more rapidly compared to that at the flame front.

For all methane flames we compare the largest absolute LIF signal levels that can be generated by ns- and ps-excitation schemes at the limit of no observable distortion in the shape of the LIF profile. This condition corresponds to the profile with the second smallest laser energy (light-blue curve) in Figures 3 and 4. However, it should be noted that LIF profiles for a few of other laser energies in between the two smallest energy values shown were recorded during the experiment, and all profiles overlap to within the measurement noise. The laser fluence and peak signal level for

the "interference-free" ns- and ps- excitation schemes are shown in Table 4. The signal levels that are listed correspond to the peak counts per laser shot that are collected roughly from a volume of (125-μm)^3 in the flame. We estimated these signal levels by integrating over a region of 5 pixels in the radial direction of the LIF line profile at the peak signal location. This corresponds to a radial distance of 125-μm and the full-width at half maximum (FWHM) of the line image in vertical direction was also approximately 125-μm. The results in Table 4 demonstrate that, except for the richest methane flame (ϕ = 1.8), the ps-excitation scheme can generate significantly higher LIF signals than the ns-excitation scheme for interference-free detection.

Table 4: Peak interference-free signal levels using ns and ps excitation in methane flames.

	Nanosecond Excitation		Picosecond Excitation	
Φ	Fluence (mJ/cm^2)	LIF (ave. cts./shot)	Fluence (mJ/cm^2)	LIF (ave. cts./shot)
0.5	0.063	40	0.015	135
0.7	0.067	57	0.039	558
1.0	0.072	111	0.041	972
1.2	0.115	289	0.160	10,400
1.5	0.155	450	0.080	3,460
1.8	0.201	872	0.038	552

3.2 Hydrogen Flames

We also investigated the ns- and ps-excitation schemes for TP-LIF detection of atomic hydrogen in a series of H_2/O_2 and $H_2/O_2/N_2$ (H_2/Air) flames covering a wide array of flame temperatures. The adiabatic flame temperature in the H_2/O_2 flames vary between approximately 2500 K – 3000 K whereas the $H_2/O_2/N_2$ flames have flame temperatures closer to 2000 K. By eliminating the possibility of interference from hydrocarbon photolytic precursors, these flames allowed us to investigate the photolytic interference primarily due to dissociation of H_2O. Furthermore, significantly higher densities of atomic hydrogen are present in the stoichiometric and rich H_2 flames as compared to CH_4 flames, and therefore, these flames provide good experimental conditions to investigate the effects of SE on TP-LIF detection of atomic hydrogen.

Relative atomic-hydrogen profiles measured in two H_2/O_2 flames (ϕ = 0.25 and 1.00) using ps- and ns-excitation schemes are shown in Figures 5 and 6, respectively. In the ϕ = 0.25 flame with ps-excitation, profile distortion due to photolytic interference is not evident (Figure 5). At the highest energies, however, the minor narrowing of the LIF profile is consistent with the effect of SE. For the ϕ = 0.75, 1.00, and 1.25 H_2/O_2 flames, we observe drastic narrowing of the H-atom profile as the ps-laser energy is increased, suggesting strong depletion of the excited-state population in the product region by SE. Simultaneously, very strong SE signals are detected at the highest laser pulse energies in these flames. On the other hand, with ns excitation, the relative H-atom profiles in all H_2/O_2 flames experience only a slight distortion at the highest laser energies. As observed in CH_4 flames previously, this small change in the profile shape is consistent with the production of atomic hydrogen via photodissociation of H_2O on the products side of the flames.

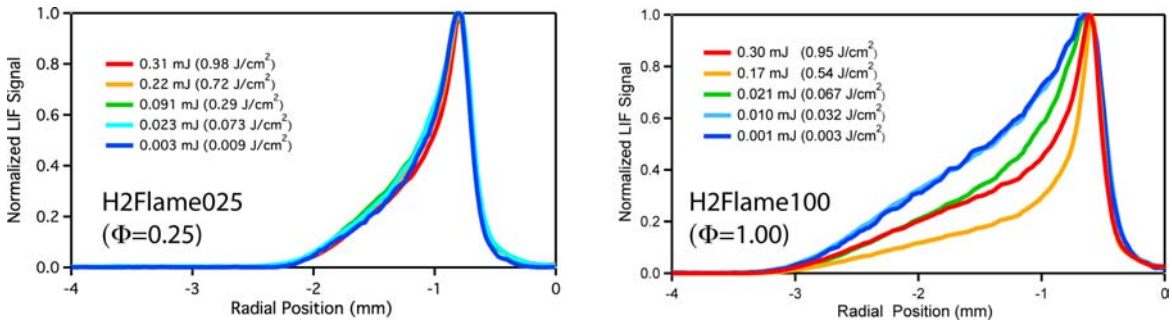

Figure 5: Hydrogen/Oxygen Flames - Picosecond Excitation Scheme

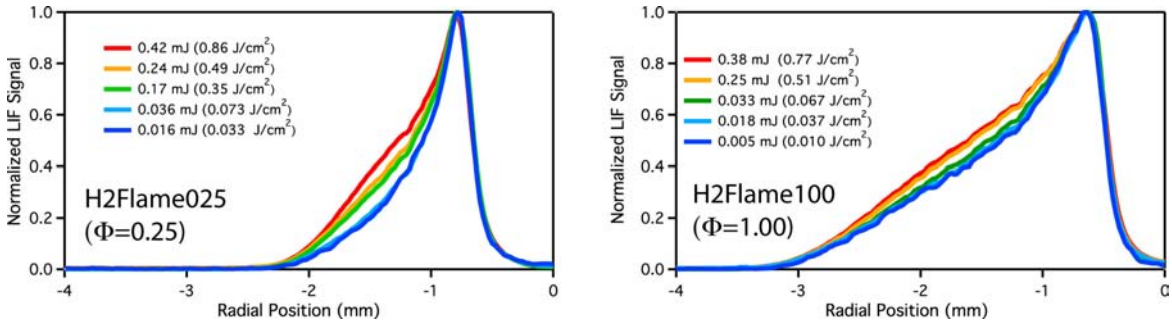

Figure 6: Hydrogen/Oxygen Flames - Nanosecond Excitation Scheme

For relatively cooler $H_2/O_2/N_2$ flames, the photolytic interferences are nearly negligible for the range of ns-laser energies used. On the other hand, profiles distortions, possibly resulting from SE, are seen in the ps-excitation scheme. Two-representative cases for the ps- and ns-excitation schemes in the stoichiometric $H_2/O_2/N_2$ flame are shown in Figure 7. Furthermore, it appears that the photolytic production of H-atoms from the vibrationally-excited water vapor is not significant in this relatively cooler $H_2/O_2/N_2$ flames.

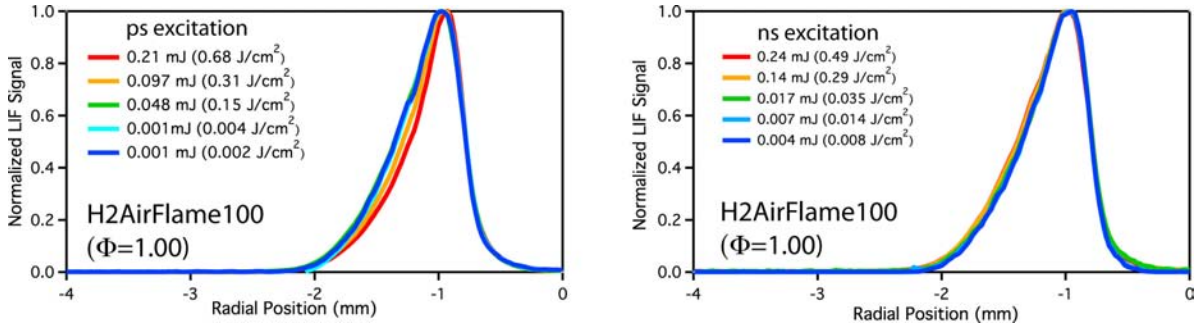

Figure 7: Hydrogen/Air Flames - Picosecond and Nanosecond Excitation Schemes

Similar to the methane flames, in these H_2 flames we compare the largest absolute LIF signal levels that can be generated by ns- and ps- excitation schemes while producing no observable

distortions in the shape of the LIF profiles. This condition corresponds to the profile with the second smallest laser energy (light-blue curve) in Figure 7. The laser fluences and peak signal levels for the interference-free ns- and ps- excitation schemes are shown in Table 5. Similar to the methane flames case, the signal levels that are listed correspond to the peak counts per laser shot that are collected roughly from a (125-μm)^3 volume in the flame. The results in Table 5 demonstrate a significant advantage to ps-excitation scheme in all H_2/O_2 flames. However, in relatively cooler $H_2/O_2/N_2$ flames, the ns-excitation scheme can produce equal or better results as compared to ps-excitation scheme.

Table 5: Peak interference-free signal levels using ns and ps excitation in hydrogen flames.

	Nanosecond Excitation		Picosecond Excitation	
Φ	Fluence (mJ/cm^2)	LIF (ave. cts./shot)	Fluence (mJ/cm^2)	LIF (ave. cts./shot)
H_2/O_2				
0.25	0.073	220	0.716	66,500
0.75	0.070	976	0.144	26,300
1.0	0.067	1,230	0.032	13,100
1.25	0.167	7,950	0.029	17,100
$H_2/O_2/N_2$				
0.62	0.492	16,200	0.073	14,900
1.0	0.489	30,400	0.152	4,460

4 Conclusions

Nanosecond- and picosecond-excitation schemes for the 205-nm, TP-LIF detection of atomic hydrogen were investigated for a range of methane and hydrogen flames. The peak laser fluences for interference-free imaging of relative atomic hydrogen profiles were determined by observing the peak-normalized, H-atom LIF profiles obtained in an axi-symmetric flame. It was found that ps-excitation scheme can produce significantly higher LIF signals at the interference-free detection limit as compared to the ns-excitation scheme in most $CH_4/O_2/N_2$ flames. Photolytic production of hydrogen atoms on the products side of the flame was attributed to photodissociation of water vapor, Hydrogen atoms created by photodissociation of CH_3 radical may be the principal cause of interference in the vicinity of the flame front. In rich $CH_4/O_2/N_2$ flames, with ps-excitation, certain distortion of the relative atomic hydrogen LIF profiles may occur due to SE.

Two types of hydrogen flames were also investigated. In relatively hot H_2/O_2 flames, ps-excitation produces higher interference-free LIF signal all flames. In rich H_2/O_2 flames, ps-excitation can generate very intense SE emission signals, causing rapid loss of excited-state population and hence significantly distorting the LIF profiles. There is evidence for certain amount hydrogen-atom creation by water vapor photodissociation when using ns-excitation scheme in these flames. In relatively cooler $H_2/O_2/N_2$ flames, ps-excitation scheme is comparable to ns-excitation scheme in lean conditions whereas the latter may be more advantages in stoicheometric $H_2/O_2/N_2$ flames.

Funding for this research was provided by the U.S. Department of Energy, Office of Basic Energy Sciences, Division of Chemical Sciences, Geosciences, and Biosciences. Sandia is a multiprogram laboratory operated by Sandia Corporation, a Lockheed Martin Company, for the U.S. Department of Energy's National Nuclear Security Administration under contract DE-AC04-94AL85000.

References

[1] R. P. Lucht, J. T. Salmon, G. B. King, D. W. Sweeney, and N. M. Laurendeau. *Opt. Lett.*, 8 (1983) 365–367.

[2] M. Alden, A. L. Schawlow, S. Svanberg, W. Wendt, and P. L. Zhang. *Opt. Lett.*, 9 (1984) 211–213.

[3] J. E. M. Golsmith and N. M. Laurendeau. *Opt. Lett.*, 15 (1990) 576–578.

[4] J. E. M. Golsmith and L. A. Rahn. *Opt. Lett.*, 15 (1990) 814–816.

[5] J. Bittner, K. Kohse-Hoingahaus, U. Meier, S. Kelm, and T. Just. *Combust. Flame*, 71 (1988) 41–50.

[6] K. E. Bertagnolli, R. P. Lucht, and M. N. Bui-Pham. *J. App. Phys.*, 83 (1998) 2315–2326.

[7] W. D. Kulatilaka, R. P. Lucht, S. F. Hanna, and V. R. Katta. *Combust. Flame*, 137 (2004) 523–537.

[8] W. D. Kulatilaka, R. P. Lucht, S. Roy, J. R. Gord, and T. B. Settersten. *Appl. Opt.*, 46 (2007) 3921–3927.

[9] J. E. M. Golsmith. *J. Opt. Soc. Am. B*, 6 (1989) 1979–1985.

[10] J. E. M. Golsmith. *Appl. Opt.*, 28 (1989) 1206–1213.

[11] K. Kohse-Hoingahaus. *Prog. Energy Combust. Sci.*, 20 (1994) 203–279.

[12] J. W. Daily. *Proc. Energy Combust. Sci.*, 23 (1997) 133–199.

[13] U. Czarnetzki, K. Miyazaki, T. Kajiwara, K. Muraoka, M. Maeda, and H. F. Dobele. *J. Opt. Soc. Am. B*, 11 (1994) 2155–2162.

[14] A. C. Eckbreth. *Laser Diagnostics for Combustion Temperature and Species*. Gordon and Breach Publishers, second edition, 1996.

[15] J. E. M. Golsmith. *Opt. Lett.*, 11 (1986) 416–418.

[16] L. Gasnot, P. Desgroux, J. F. Pauwels, and L. R. Sochet. *Appl. Phys. B*, 65 (1997) 639–646.

[17] R. Quandt, X. Wang, Z. Min, H. L. Kim, and R. Bersohn. *J. Phys. Chem.*, 102 (1998) 6063–6067.

[18] J. E. M. Golsmith, M. Alden, and U. Westblom. *Appl. Opt.*, 29 (1990) 4852–4859.

[19] J. H. Frank and T. B. Settersten. *Proceedings of the Combustion Institute*, 30 (2005) 1527–1534.

[20] T. B. Settersten, A. Dreizler, B. D. Patterson, P. E. Schrader, and R. L. Farrow. *Appl. Phys. B*, 76 (2003) 479–482.

[21] J. H. Frank, X. Chen, B. D. Patterson, and T. B. Settersten. *Appl. Opt.*, 43 (2004) 2588–2597.

[22] P. P. Yaney, D. A. V. Kliner, P. E. Schrader, and R. L. Farrow. *Rev. Sci. Inst.*, 71 (2000) 1296–1305.

[23] P. Desgroux, L, B. Crunelle, and J. F. Pauwels. *Proceedings of the Combustion Institute*, 26 (1996) 967–974.